Carbohydrate Polymers 101 (2014) 392–400

Contents lists available at ScienceDirect

Carbohydrate Polymers

journal homepage: www.elsevier.com/locate/carbpol

Porous graphene oxide/carboxymethyl cellulose monoliths, with high metal ion adsorption

Yongli Zhang [a], Yue Liu [b,*], Xinrui Wang [b], Zhiming Sun [a], Junkui Ma [b], Tao Wu [b], Fubao Xing [b], Jianping Gao [b]

[a] Huanhu Hospital, Tianjin 300060, PR China
[b] School of Science, Tianjin University, Tianjin 300072, PR China

ARTICLE INFO

Article history:
Received 14 June 2013
Received in revised form 6 September 2013
Accepted 18 September 2013
Available online 30 September 2013

Keywords:
Graphene oxide
Carboxymethyl cellulose
Porous monolith
Metal ion adsorption

ABSTRACT

Orderly porous graphene oxide/carboxymethyl cellulose (GO/CMC) monoliths were prepared by a unidirectional freeze-drying method. The porous monoliths were characterized by Fourier transform infrared spectra, X-ray diffraction and scanning electron microscopy. Their properties including compressive strength and moisture adsorption were measured. The incorporation of GO changed the porous structure of the GO/CMC monoliths and significantly increased their compressive strength. The porous GO/CMC monoliths exhibited a strong ability to adsorb metal ions, and the Ni^{2+} ions adsorbed on GO/CMC monolith were reduced by $NaBH_4$ to obtain Ni GO/CMC monolith which could be used as catalyst in the reduction of 4-nitrophenol to 4-aminophenol. Since CMC is biodegradable and non-toxic, the porous GO/CMC monoliths are potential environmental adsorbents.

1. Introduction

Foams that are ultra-light and highly porous are typically manufactured by subjecting a wet-gel precursor to critical-point lyophilization (freeze-drying) in order to remove the liquid without collapsing the network (Cervin, Aulin, Larsson, & Wågberg, 2012). The potential applications of foams include catalyst supports, catalysts, substrates for drug delivery systems, and scaffolds for tissue engineering (Gutiérrez et al., 2007; Mukai, Nishihara, Shichi, 2004; Nishihara, Mukai, & Tamon, 2004; Stokols & Tuszynski, 2004). At present, porous materials are prepared by porogenic and non-porogenic methods. Gas forming, particle leaching, and freeze-drying are typical porogenic methods, of which freeze-drying is especially attractive since water can be used as the porogen to prepare the porous materials (Chen & Ma, 2004; Ishaug-Riley, Crane-Kruger, Yaszemski, & Mikos, 1998; Lee, Kim, Chong, & Lee, 2004; Lee et al., 2005). This makes the materials useful as scaffolds for cell cultures (Stokols & Tuszynski, 2004).

Oriented pore structures are an important property for foams both from theoretical and technological application points of view (Balaji, El-Safty, Matsunaga, Hanaoka, & Mizukami, 2006; Carrington, Thomas, Rodman, Beach, & Xue, 2007; Wen et al., 2011). Recently, an ice-segregation-induced self-assembly process, also called a unidirectional freezing-drying method, was used to fabricate foams with oriented pore structures (Wen et al., 2011). At present, this is the simplest way to prepare oriented foams and this method has been exploited for preparing aligned organic foams (Stokols & Tuszynski, 2004; Yang et al., 2006; Zhang, Hussain, et al., 2005; Zhang, Long, & Cooper, 2005), inorganic foams (Devile, Saiz, Nalla, & Tomsia, 2006; Devile, Saiz, & Tomsia, 2007; Gutiérrez, Jobbágy, Rapún, Ferrer, & del Monte, 2006) and composite foams (Shunji et al., 2007; Yunoki et al., 2006). These novel hierarchical porous systems are suitable for a wide range of advanced applications (Darder et al., 2011), including cell culture, drug delivery and chemical adsorption.

Industrial development in China has created considerable quantities of industrial waste effluents which contain significant amounts of heavy metals and/or other toxic species. These effluents have detrimental impacts on both the environment and the health of people (Wang et al., 2012). Several technologies are currently being developed to achieve efficient removal of these toxic species such as ion exchange, adsorption, and membrane processes (Demirbas, 2008; Hu, Lei, Li, & Ni, 2003; Reddad, Gerente, Andres, Thibault, & Le Cloirec, 2003). Adsorption methods are simple and economical and the removal of toxic chemicals using porous adsorbents has attracted considerable attention due to the high efficiencies of these adsorbents (Wan Ngah & Hanafiah, 2008).

As the most abundant natural polymer, cellulose has been extensively studied in both theory and applications. Carboxymethyl cellulose (CMC) (the sodium salt of the carboxymethyl ether of cellulose) is an anionic polysaccharide produced from

* Corresponding author. Tel.: +86 022 27403475; fax: +86 022 27403475.
E-mail addresses: lyliuyue1990@gmail.com (Y. Liu), zhimingsuntju@126.com (Z. Sun), fbxing@suho.com (F. Xing).

0144-8617/$ – see front matter © 2013 Elsevier Ltd. All rights reserved.
http://dx.doi.org/10.1016/j.carbpol.2013.09.066

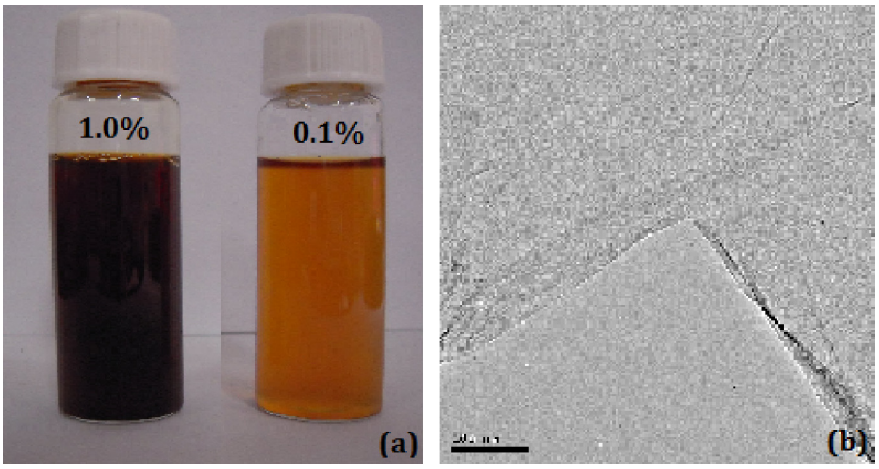

Fig. 1. Photos of aqueous suspensions of GO (1.0% and 0.1%) (a) and TEM photo of GO sheet (b).

cellulose, monochloroacetic acid and sodium hydroxide (Grzadka & Chibowski, 2012) Since it is low-cost, non-toxic, renewable, biodegradable and modifiable (Ali, El-Rehim, Kamal, & Hegazy, 2008), CMC is considered a biocompatible material and used in drug delivery and tissue enginering. It is also an effective adsorbent for the removal of metal ions because it contains numerous active functional groups including hydroxyl and carboxyl groups which can chelate with metal ions and interaction with organic compounds.

Since adsorption depends on surface area, adsorbents are usually prepared as porous structures or nanoparticles (Zhang, Qiu, Si, Wang, & Gao, 2011). Therefore, the adsorption capacity of CMC should be improved if it is fabricated into a highly porous structure. However, highly porous structures make materials unstable, so cross-linking is often used to improve the strength of the material. But this reduces the adsorption capacity (Q_e) for metal ions because cross-linking reactions consume the functional groups which are need to interact with the metal ions (Matos & Arruda, 2003).

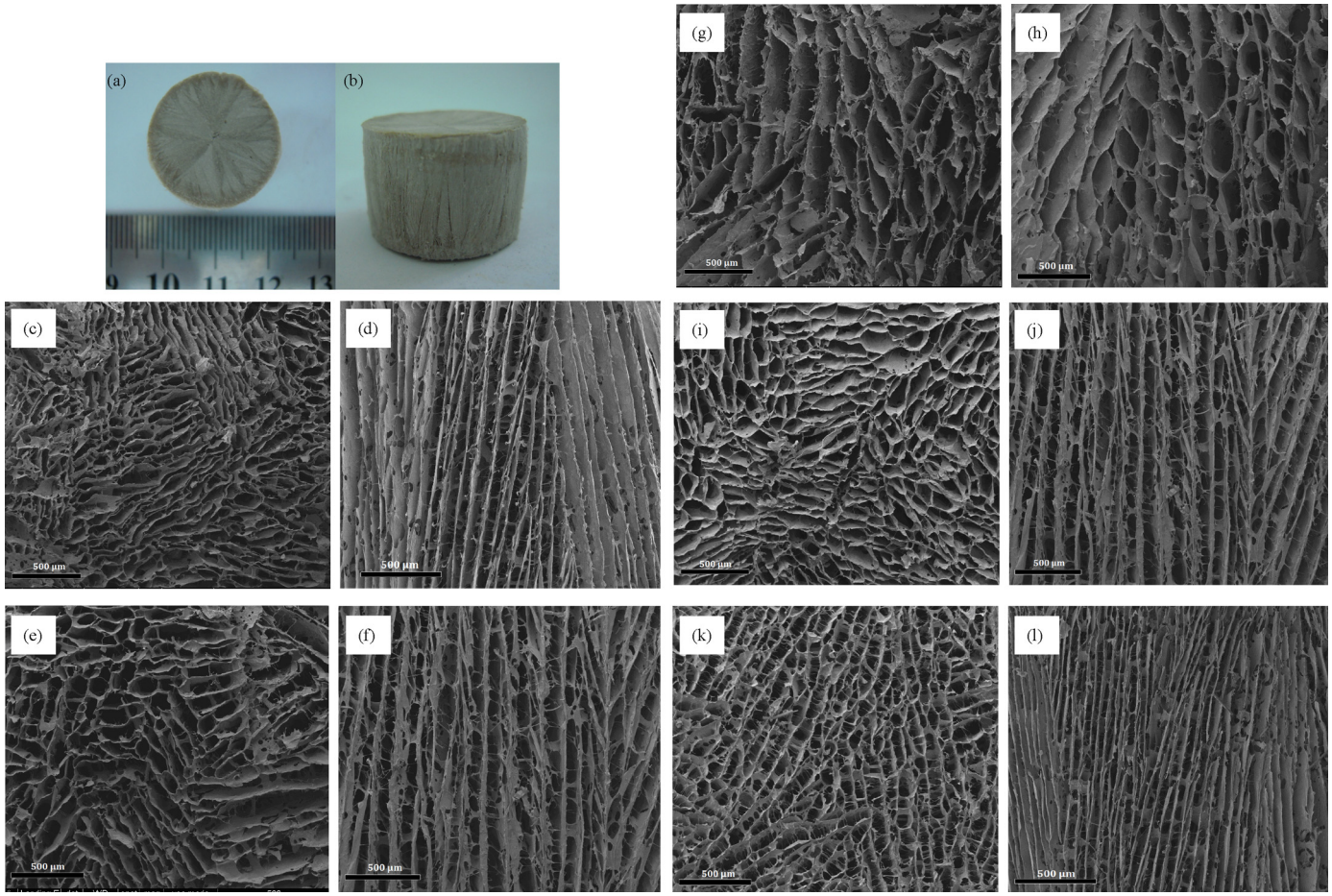

Fig. 2. Photographs of porous GO/CMC monoliths (a, b), SEM photos of porous GO/CMC monoliths with 2 wt% CMC and different GO concentrations [0 wt% GO (c, d); 1.0 wt% GO (e, f); 3.0 wt% GO (g, h)], and SEM of porous CMC/GO monoliths with 1.0 wt% GO and different CMC concentrations [3 wt% CMC (i, j); 6 wt% CMC (k, l)].

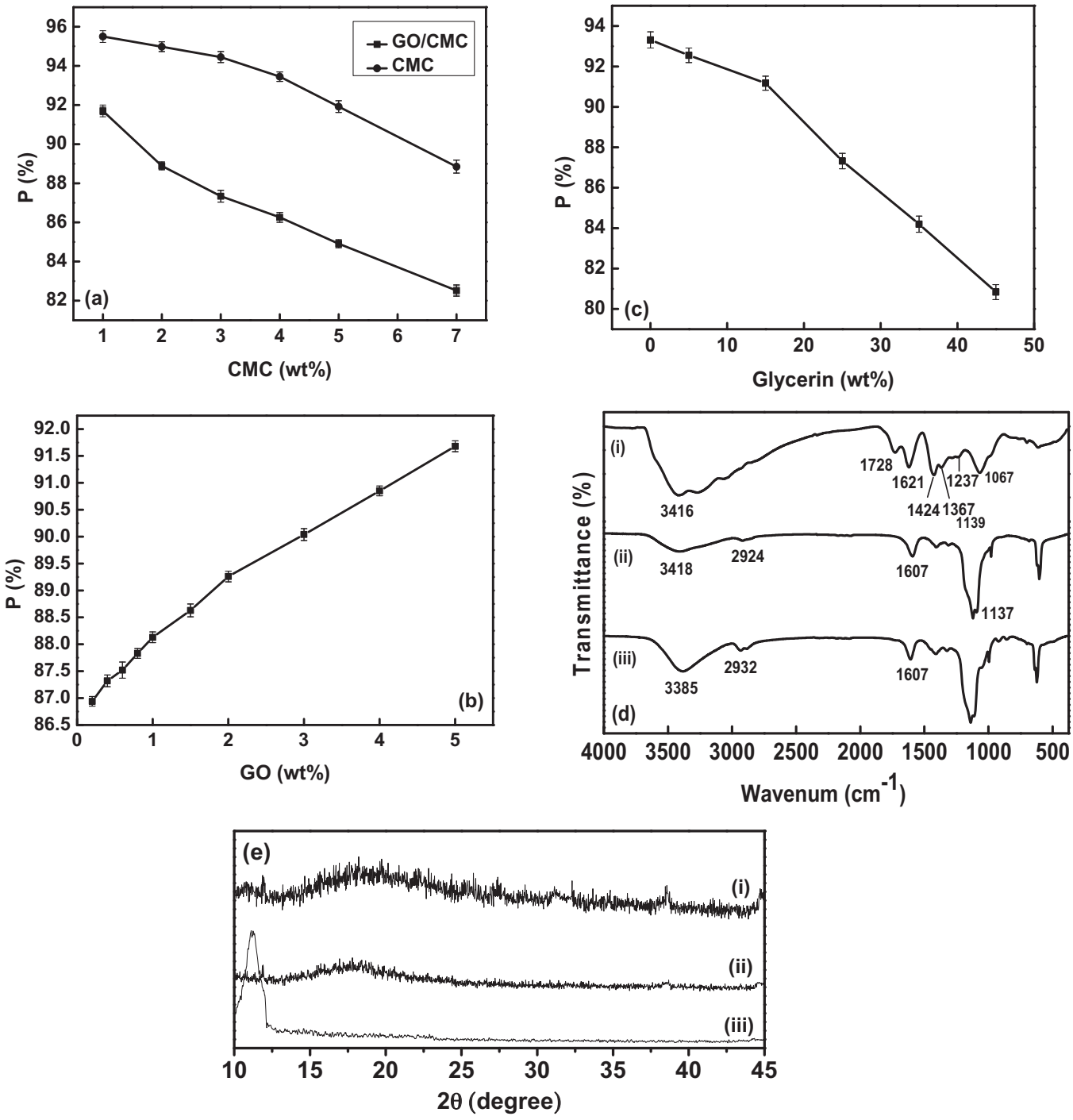

Fig. 3. Porosity of the CMC (25 wt% glycerin) and GO/CMC (0.6 wt% GO and 25 wt% glycerin) monoliths with different CMC concentrations (a); porosity of the GO/CMC (4 wt% CMC and 25 wt% glycerin) with different GO concentrations (b), and porosity of the GO/CMC (4 wt% CMC and 0.6 wt% GO) with different glycerin concentrations (c), IR of spectra (d) of GO (i), porous GO/CMC monolith with 4 wt% CMC and 1.0 wt% GO (ii), and CMC (iii), XRD diagrams (e) of GO/CMC with 1.0 wt% GO (i), CMC (ii) and GO (iii).

Another effective way to improve the strength of a material is to add reinforcing fillers. Graphite oxide, an oxygen-rich carbonaceous layered material, is produced by the oxidation of graphite (Zhang et al., 2011). Graphite oxide exhibits an extended layered structure with hydrophilic polar groups (—OH, —COOH, —CHO, and epoxy groups) protruding from its layers, which results in interesting swelling, intercalating and ion exchange properties (Dikin et al., 2007). Each layer of graphite oxide is essentially an oxidized graphene sheet commonly referred to as graphene oxide (GO). Recently, GO has gained considerable attention as a significant component of new composite materials (Soldano, Mahmood, & Dujardin, 2010). Its huge surface area endows it with strong adsorption abilities much like carbon nanotubes (Seredych & Bandosz, 2009; Zhang, Huang, Yang, & Kang, 2008). Therefore, the addition the GO/CMC monoliths were fabricated and used as adsorbents for metal ions. GO should enhance not only the strength but also the adsorption ability of porous GO/CMC monoliths. In this paper, GO/CMC monoliths were fabricate by freeze-drying method

and use the monoliths to absorb metal ions and then transform them into metal nanoparticles that can catalyze the reduction of 4-nitrophenol (4-NP) to 4-aminophenol (4-AP). So the polluters, metal ions, are not only removed from the polluted water and also turn to useful catalyst.

2. Experimental

2.1. Materials

The graphiate was manufactured by Huadong Graphite Co. Carboxylmethly cellulose, glycerin, xylenol orange, methyl orange, methylene blue, the Cu^{2+}, Pb^{2+}, Cd^{2+}, Co^{2+} and Ni^{2+} standard solutions, $NaBH_4$ and 4-nitrophenol (4-NP) were all from Tianjin Chemical Reagent Co.

2.2. Preparation of GO

Graphene oxide was prepared from purified natural graphite by a modified Hummer's method (Hummers & Offeman, 1958). Briefly, concentrated H_2SO_4 (25 mL) was added to a 250-mL flask filled with graphite (1 g), followed by the addition of $NaNO_3$ (0.8 g), and then solid $KMnO_4$ (2.5 g) was gradually added with stirring while the temperature of the mixture was kept below 20 °C for 2 h. Next the temperature was increased to 30 °C and then excess distilled water was added to the mixture and the temperature was then increased to 80 °C and stirred for 0.5 h. Finally, 30% H_2O_2 was added until the color of mixture changed to brilliant yellow. The mixture was filtered and the filter cake was washed several times with 5% aqueous HCl to remove metal ions and then it was washed with distilled water to remove the acid. The resulting filter cake was dried in air then re-dispersed into water. The GO suspension was obtained after 3 h of ultrasonic treatment.

2.3. Preparation of porous GO/CMC and CMC monoliths

A weighed amount of CMC was added to distilled water and stirred to form a CMC solution. The CMC solution was then added to the GO suspension with stirring, followed by ultrasonic treatment in an ice bath for about 10 min. This produced a GO/CMC suspension. Three series of samples were prepared: series 1 is GO/CMC suspensions with different weight percentages of CMC (2%, 3%, 4%, 5% and 7%) and fixed amounts of GO and glycerin; series 2 has different weight percentages (relative to the weight of CMC) of GO (0.2%, 0.6%, 0.8%, 1.0% 1.5%, 2.0%, 3.0%, 4.0% and 5.0%); and series 3 has different weight percentages (relative to the weight of CMC) of glycerin (5%, 15%, 25%, 35% and 35%).

The GO/CMC suspension gel was injected into a plastic tube (20-mm in diameter and 50-mm in length) that was placed in an insulated Styrofoam container, with only the bottom surface of the plastic tube exposed. The Styrofoam container was placed on top of a 6-cm diameter metal disk, which in turn rested on a 6-cm-deep pool of liquid nitrogen to create a uniaxial thermal gradient (Dikin et al., 2007). As the liquid nitrogen evaporated, the mixture was unidirectionally frozen from bottom to the top. The solidified mixture was then transferred to a freeze-drying vessel (Alphal1-2, Christ, Germany) and freeze-dried at −50 °C for 48 h under vacuum (less than 20 Pa) to obtain the porous GO/CMC monoliths. Similarly, porous CMC monoliths were prepared with no GO. The porous monoliths were stored in a desiccator for further analysis.

2.4. Scanning electron microscopy (SEM) of the porous GO/CMC monoliths

The morphologies of the porous GO/CMC monoliths were observed with a scanning electron microscope (Nanosem430, FEI, USA). The samples were gold coated using a sputtering coater (Desk-II; Denton Vacuum, USA) before observation.

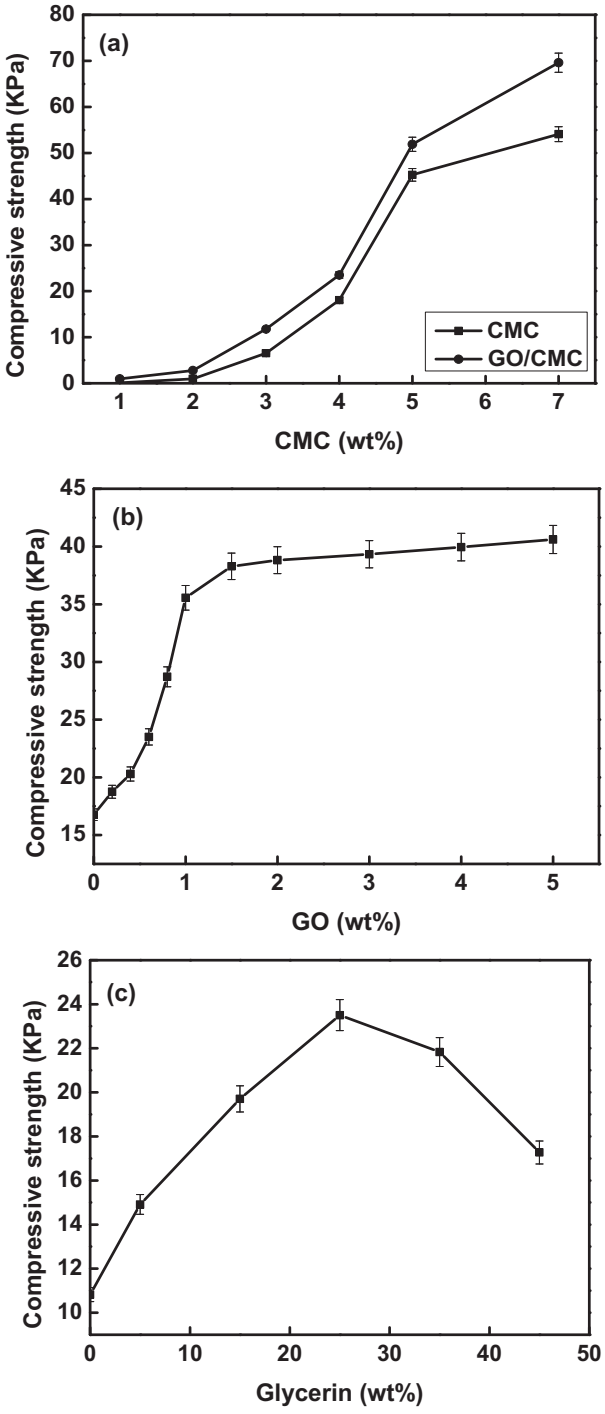

Fig. 4. Compressive strength of the porous CMC and GO/CMC (0.6 wt% GO) monoliths with 25 wt% glycerin and different CMC concentrations (a); GO/CMC monoliths with 4 wt% CMC, 25 wt% glycerin and different GO concentrations (b); GO/CMC monoliths with 4 wt% CMC, 0.6 wt% GO and different glycerin concentrations (c).

2.5. Fourier transform infrared spectra (FT-IR) of the GO/CMC

A Fourier transform infrared spectrometer (Paragon-1000, Perkin-Elmer, USA) was used to characterize the GO/CMC samples. The GO, CMC and GO/CMC powders were pulverized with KBr and pressed into pellets. The spectra were obtained in the range of

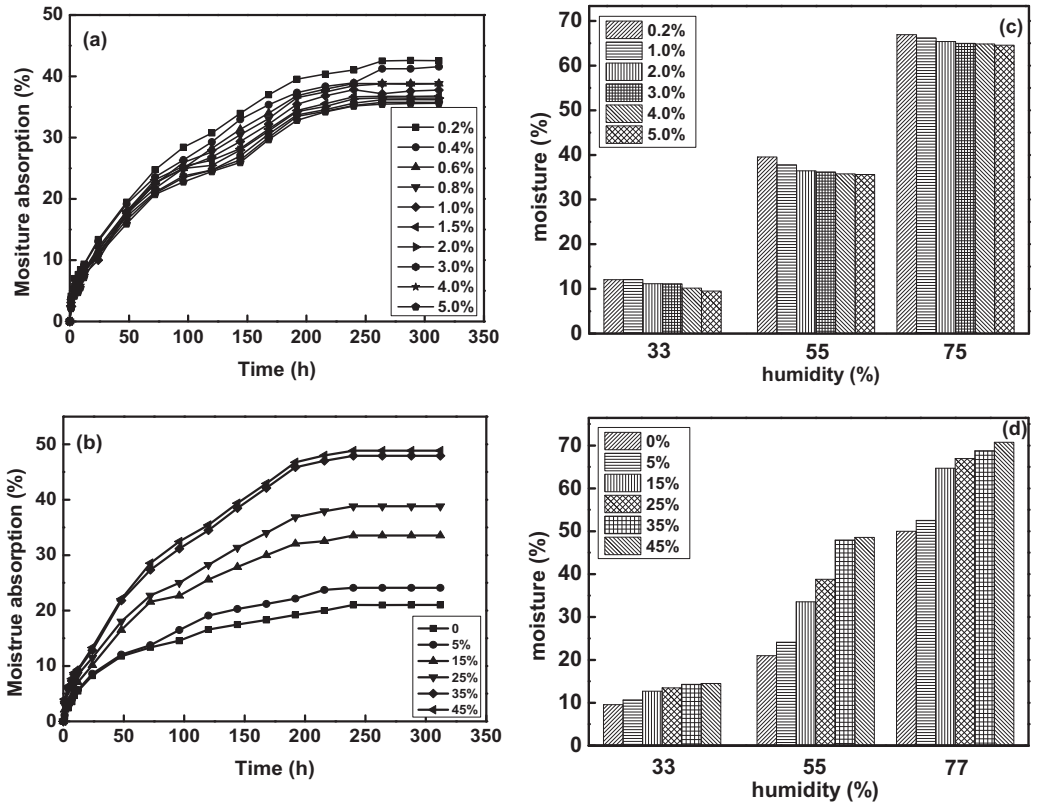

Fig. 5. Moisture adsorption of the porous GO/CMC monoliths (4 wt% CMC, 25 wt% glycerin) with different GO at RH = 55% (a), moisture adsorption of the porous GO/CMC monoliths (4 wt% CMC, 0.6 wt% GO) with different glycerin concentrations at RH = 55% (b), moisture adsorption of the porous GO/CMC monoliths (4 wt% CMC, 25 wt% glycerin) with different GO concentrations at different RH (c), and moisture adsorption of the porous GO/CMC monoliths (4 wt% CMC, 0.6 wt% GO) with different glycerin concentrations at different RH (d).

500–4000 cm^{-1} by averaging 16 scans at 1 min intervals to minimize the effects of dynamic scanning. The resolution was 4 cm^{-1}.

2.6. X-ray diffraction (XRD) analysis

The elemental compositions of GO, CMC and GO/CMC were determined using X-ray photoelectron spectroscopy (PHI1600 ESCA System, Perkin Elmer, USA) at 300 K by step scanning, with a Cu Kα tube at 36 kV and 20 mA.

2.7. Porosity of the porous GO/CMC monoliths

The porosity of the porous CMC/GO monoliths was calculated according to the following equation:

$$\text{Porosity}\ (\%) = \frac{V_t - V_a}{V_t} \times 100 = \frac{V_t - W_t/\rho}{V_t} \times 100 \quad (1)$$

where V_t (cm^3) is the total volume of the porous GO/GO monoliths, V_a (cm^3) is the actual volume of the material, W_t (g) is the mass of the monoliths, and the ρ (g cm^{-3}) is the density of the material. Each sample was measured in triplicate and the average value was calculated.

2.8. Compressive strength of the porous GO/CMC monoliths

The compressive strengths of the porous GO/CMC monoliths were measured by placing the samples into a programmable temperature and humidity chamber with a temperature of 25 ± 2 °C and an atmosphere of 65 ± 2% relative humidity (RH) for about 24 h. Then the compressive strengths of the sample, along the longitudinal and transverse directions, were measured with a dynamic mechanical analyzer at a compressing rate of 1 mm min^{-1}.

2.9. Adsorption of the porous GO/CMC monoliths for heavy metal ions

A weighed amount of the porous GO/CMC monolith was put into a 250-mL comical flask containing 250 mL of metal ion solution and the monolith was allowed to adsorb at room temperature. The solution contained equal concentrations of Cu^{2+}, Pb^{2+}, Cd^{2+}, Co^{2+} and Ni^{2+} and solutions with different total concentrations (40, 60, 80, 100 and 120 mg L^{-1}) were tested. After adsorption was complete, the monolith was removed and the concentrations of the metal ions were measured using an inductively coupled plasma optical emission spectrometer (ICP-OES, Vista-MPX, Varian) with a high frequency emission power of 1.5 kW and a plasma air flow of 15.0 L min^{-1}.

The adsorption capacity (Q_e) and adsorption efficiency (Abe) of the porous monolith were calculated according to following equations.

$$Q_e = \frac{(C_0 - C_e)V}{W} \quad (2)$$

$$\text{Abe}\,(\%) = \frac{C_0 - C_e}{C_0} \times 100 \quad (3)$$

where C_0 (mg L^{-1}) denotes the initial concentration of the metal ions, C_t (mg L^{-1}) is the equilibrium concentration, V (L) is the volume of the solution, and W (g) is the weight of the porous GO/CMC monolith.

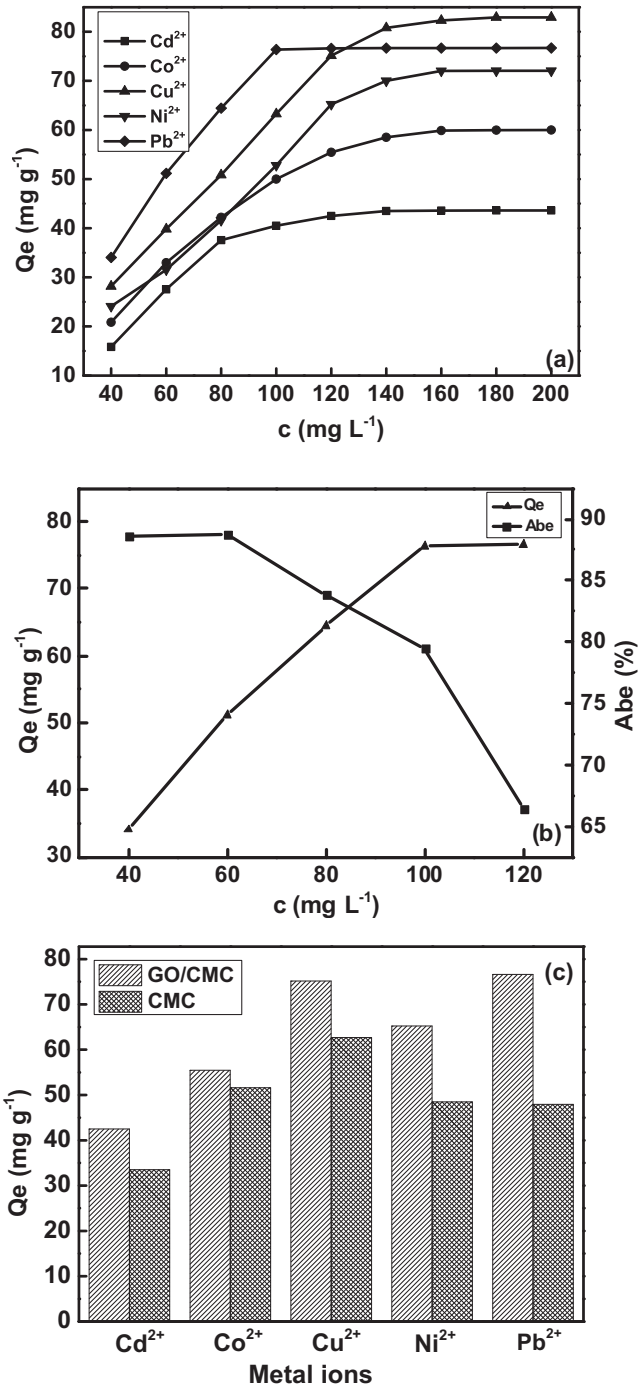

Fig. 6. Adsorption capacity of the GO/CMC monoliths for different concentrations of metal ions (a); adsorption capacity and adsorption efficiency of the GO/CMC monoliths for different concentrations of Pb^{2+} (b); adsorption capacity of CMC and GO/CMC for metal ions with a concentration of 120 mg L^{-1} (c).

2.10. Preparation of Ni loading GO/CMC monolith (Ni@GO/CMC) for the reduction of 4-NP

The Ni^{2+} adsorbed CMC/RGO monolith in the above experiment was kept in distilled water for 12 h to remove unbound Cu^{2+}, and then it was soaked in 50 mL 0.5 M $NaBH_4$ solution and stayed for 1 h at 25 °C to allow the reduction of Ni^{2+} to Ni nanoparticles. The Ni@GO/CMC was washed with distilled water, freeze-dried for 48 h. Then, the Ni@GO/CMC was added to aqueous 4-NP solution consisting of 0.015 M 4-NP and 0.5 M $NaBH_4$ to initiate the reduction of 4-NP to 4-AP. The conversion of the reduction was measured by the change in intensity of 4-NP at 400 nm by employing a UV–vis spectrophotometer.

3. Results and discussion

3.1. Characterization of the porous GO/CMC monoliths

Fig. 1 shows the photos and TEM image of the aqueous suspensions of GO that were used to prepare the porous GO/CMC monoliths. The monoliths were prepared in our laboratory and characterized with Raman, XPS and other methods (Li et al., 2012). The exfoliated GO readily dispersed in water with mild ultrasonic treatment and formed a transparent suspension that was stable for several months. The TEM photo demonstrates that the GO sheets consist of one to several layers. The well dispersed GO suspension is useful for preparing GO/CMC solutions and porous GO/CMC monoliths.

Fig. 2 shows photographs of the porous GO/CMC monoliths. The GO/CMC monoliths have a radial appearance on top and have vertical lines down the sides (Fig. 2a and b). This indicates an ordered porous architecture which can clearly be seen in the SEM photos. The SEM images of the cross-sections (left) and vertical-sections (right) of the porous GO/CMC monoliths with different GO and CMC concentrations are shown in Fig. 2c–l. Clearly the pore diameters increase significantly as the GO concentration increases (Fig. 2c–h), but they decrease as the CMC concentration increases (Fig. 2i–k). In all the monoliths, there are many "micro-ribbons" protruding from the pore walls. This phenomenon is more prominent at higher GO concentration, and eventually, the "micro-ribbons" form adjacent walls which connect and divide the long pore into several parts (Fig. 2k and l).

The porous GO/CMC monoliths were formed during freeze drying and ice crystals were used as porogens. When GO was added, the CMC solution became viscous, so the ice crystals could not easily keep the two materials completely separated and "micro-ribbons" were formed. These "micro-ribbons" may play a role in improving the compressive strength of the porous monoliths.

The GO/CMC monoliths are lightweight and full of pores. Fig. 3 shows the relationship between the porosity of the GO/CMC monoliths and the CMC concentration, glycerin and GO contents. The porosity of all the monoliths is more than 80% and the highest porosity of 96% was seen for the monolith made from wt% CMC solution.

As seen in Fig. 3a, the porosities of the CMC and GO/CMC monoliths decreased as the CMC concentration increased. In addition the CMC monoliths all had higher porosities compared with the GO/CMC monoliths with the same CMC concentrations. As shown in Fig. 3b, the porosity of the porous GO/CMC monoliths increased with the increase of GO content, although the addition of more GO increased the solid mass in the monoliths. That may because the "micro-ribbons" prevented the contraction of the porous structure. The effect of glycerin content on the porosity of the GO/CMC monoliths is shown in the Fig. 3c. The porosity of the GO/CMC monoliths decreased as the glycerin content increased. This is because the addition of glycerol reduced the interactions between the macromolecules which made the porous GO/CMC monoliths shrink.

Fig. 3d shows the FT-IR spectra of GO, GO/CMC and CMC. The FT-IR spectrum of GO contains a broad band at 3416 cm^{-1}, which is related to the —OH groups, and bands at 1728 and 1621 cm^{-1} from the carboxyl and C=C groups respectively. Other bands at 1367 cm^{-1} (C—OH), 1237 cm^{-1} (C—O—C) and 1067 cm^{-1} (C—O) are also seen. These characteristic peaks indicate that GO have been successfully synthesized.

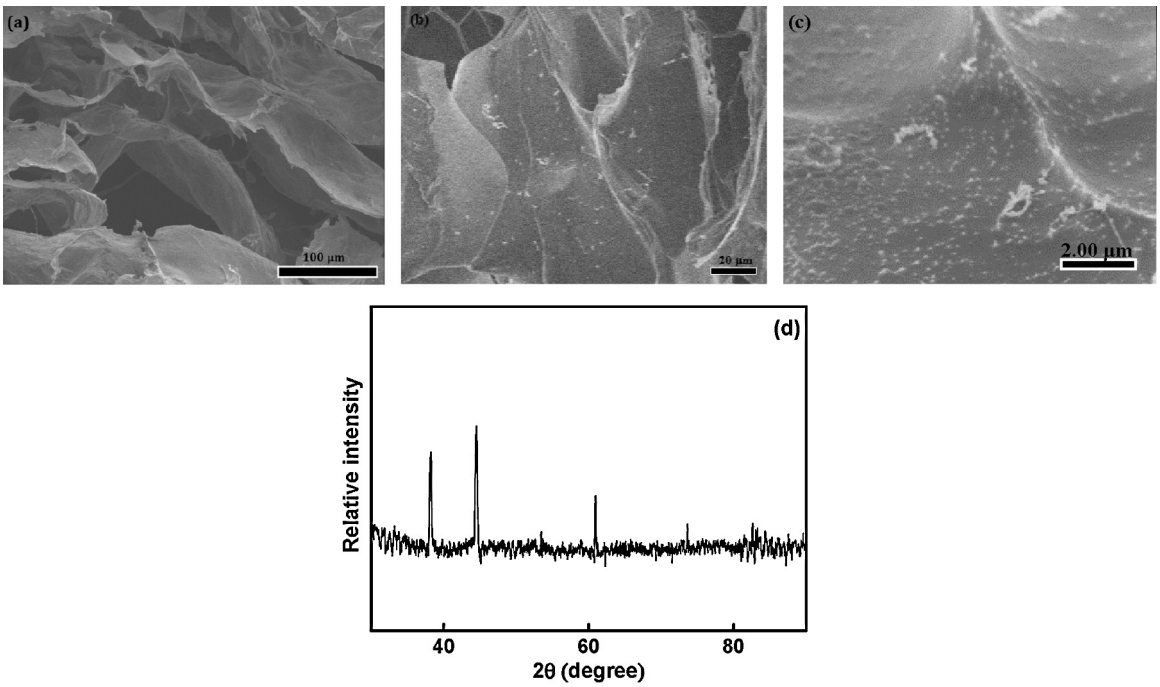

Fig. 7. SEM photos (a, b and c) and XRD pattern (d) of the Ni@GO/CMC.

Fig. 3d (iii) shows the characteristic adsorption bands of CMC at around 3418 and 1607 cm^{-1} which are due to hydroxyl stretching and carboxylate bending modes, respectively (Zohuriaan-Mehr, Pourjavadi, & Salehi-Rad, 2004). In addition, the adsorption bands at 2924 and 1137 cm^{-1} are due to the C—H stretching and bending modes, respectively (Zohuriaan-Mehr et al., 2004). The IR spectrum of the porous GO/CMC monolith (Fig. 3d (ii)) demonstrates characteristic peaks of both CMC and GO. The peak at 3385 cm^{-1} is the stretching vibration of the hydroxyl group (from both CMC and GO) and the peak at 2932 cm^{-1} is the characteristic C—H stretching of $—CH_2$ (from CMC). The IR data indicates that GO and CMC form a blend and that no chemical reactions occurred when they were combined.

To obtain information about the crystalline structure of the GO/CMC monolith, the XRD patterns of the GO, CMC and GO/CMC with 1.0 wt% GO were measured and are shown in Fig. 3e. GO has a characteristic diffraction peak at 11.4°. This indicates that the interlayer spacing in the GO is 0.80 nm which is larger than that in graphite. The CMC has a broad diffraction peak at 17°, indicating that CMC is partly crystalline. The CMC/GO has a very small peak in 11.4° and an obvious diffraction peak at about 17°. Overall, the XRD diagram of GO/CMC is similar to CMC because the GO content is too small to produce much of a peak.

3.2. Compressive strength of porous GO/CMC monoliths

Compressive strength is one of the most important parameters used to evaluate porous materials. Fig. 4 illustrates the effects of CMC (a), GO (b) and glycerin (c) concentration on the compressive strength of the porous GO/CMC monoliths. Fig. 4a shows the compression strength of the GO/CMC monoliths increased with the CMC concentration increasing. That may because the pore wall in the GO/CMC monoliths became thicker as the CMC concentration increased. The compressive strength of GO/CMC reached 70 kPa when the CMC concentration was 7 wt%.

When the GO content was less than 1.0 wt%, the compressive strength of the monoliths increased rapidly with increasing GO content (Fig. 4b). However, a maximum was reached at 1.0 wt% and further increasing the amount of GO did not result in an obvious improvement in the compressive strength. Therefore monoliths with 1 wt% GO were used in the subsequent experiments.

Fig. 4c demonstrates the relationship between the compressive strength of GO/CMC and the glycerin content. The compressive strength reached a maximum value when the glycerin content was 25 wt%. Glycerin can increase the flexibility of the CMC, so at lower concentrations the compressive strength increased when it was added since the GO/CMC monolith is not easily broken under a load. However, glycerol also reduces macromolecular interactions which decrease the compressive strength. So the GO/CMC monolith loading with 25 wt% glycerin was the optimal balance of these two factors and gave the highest compressive strength.

3.3. Moisture adsorption by the porous GO/CMC monoliths

CMC readily adsorbs moisture because CMC macromolecules contain many carboxyl and hydroxyl groups. The moisture adsorption of the porous CMC and GO/CMC monoliths at RHs of 33%, 55%, and 81% were tested and the results are given in Fig. 5 For all the porous CMC and GO/CMC monoliths, the moisture adsorption increased with time until a maximum value (MA_{max}) was reached (Fig. 5a and b). The moisture adsorption of the porous GO/CMC monoliths was lower than that of the porous CMC monoliths. When the GO loading was 5.0 wt%, the monoliths had the lowest moisture adsorption. These results suggest that the addition of GO improves the resistance of the porous GO/CMC monoliths to water.

As shown in Fig. 5b, the moisture adsorption of the porous GO/CMC monoliths increased as the glycerol concentration increased. This is because glycerol has excellent water-retaining ability. In addition, as shown Fig. 5c and d, the GO/CMC monoliths have larger MA_{max} values under high RH conditions. For a given RH value, the MA_{max} values do not change obviously with GO content, whereas, the amount of glycerin has a significant effect on the MA_{max} values. The GO/CMC monoliths loaded with more glycerin have larger MA_{max} values (Fig. 5d).

3.4. Adsorption of heavy metal ions by the porous GO/CMC monoliths

Fig. 6 shows the adsorption of metal ions by the porous GO/CMC and CMC monoliths. Fig. 6a shows the adsorption capacity of the porous GO/CMC monolith (4 wt% CMC, 1 wt% GO and 25 wt% glycerin) for different concentrations of different metal ions in aqueous media. For all the ions, the Q_e increased as the ion concentration increased, but the Q_e value was different for each ion and was in the order of Cu^{2+} (82.93 mg g^{-1}) > Pb^{2+} (76.70 mg g^{-1}) > Ni^{2+} (72.04 mg g^{-1}) > Co^{2+} (59.99 mg g^{-1}) > Cd^{2+} (46.13 mg g^{-1}).

The effect of the Pb^{2+} concentration on the adsorption is shown in Fig. 6b. As the Pb^{2+} concentration increased, the Q_e rapidly increased until it reached a maximum value of 76.6 mg g^{-1} for Pb^{2+} concentrations over 100 mg L^{-1}. In contrast, the Ade gradually decreased as the Pb^{2+} concentration increased. These trends can be readily understood. At high Pb^{2+} concentrations, more ions are adsorbed onto the porous GO/CMC monoliths because of the adsorption–desorption equilibrium, resulting in an increase in Q_e. Simultaneously, at higher Pb^{2+} concentrations, more Pb^{2+} ions are left in the solution because the total amount of Pb^{2+} ions greatly exceeds the adsorption capacity of the porous GO/CMC, so the Ade decreases. The above phenomena were also found in the adsorption behavior of other ions by the GO/CMC monoliths.

The effect of GO on the adsorption ability of porous GO/CMC monoliths for heavy metal ions is shown in Fig. 6c. The GO/CMC monoliths have a higher adsorption capacity than the CMC monoliths. This is because the hydroxyl and carboxyl groups on the GO sheets increase the ability of the porous GO/CMC monoliths to adsorb metal ions. So the addition of GO not only mechanically reinforces the porous GO/CMC monoliths, but also increases the ability of the monoliths to adsorb metal ions.

3.5. Catalytic performance of Ni@GO/CMC for the reduction of 4-NP to 4-AP

Nitrophenols are the most common organic pollutant in industrial and agricultural waste waters, and it would be useful to develop a process for the conversion of 4-NP to 4-AP in aqueous solution under mild conditions. Previously Ni-B and Co-B have been prepared and used as catalysts in the reduction of 4-NP to 4-AP (Kim & Lee, 2004; Moon, Ko-du, Park, Joo, & Jeong, 2012). Here, the Ni^{2+} ions adsorbed onto the GO/CMC monolith were reduced to form Ni@GO/CMC which was then used as a catalyst in the reduction of 4-NP to 4-AP. Evidence for the formation of the Ni nanoparticles on the GO/CMC is seen in the SEM photos and the XRD pattern of Ni@ GO/CMC in Fig. 7. As the reduction of 4-NP started, the absorption peak at 400 nm gradually decreased in intensity with a concurrent increase in a new absorption peak at 300 nm, which indicates the formation of 4-AP. Therefore, the reduction process can be easily monitored with time-dependent UV–vis absorption spectra as shown in Fig. 8a. In the absence of the catalyst, the absorption intensity was almost unchanged after a long period of time, even with a large excess of $NaBH_4$. In contrast, after the addition of Ni@GO/CMC to the system, the absorption intensity at 400 nm decreased rapidly with time, and the reduction reaction was completed in less than one minute. As shown in Fig. 8b, the rate constant (K) was calculated to be 0.0797 s^{-1} (4.782 min^{-1}) for the reaction of 4-NP to 4-AP. This is an extremely quick reaction rate compared with that of other reported Ni-based catalysts. Bultan and Sahiner reported the reduction of 4-NP catalyzed by acrylamidoglycolic acid–Ni hydrogel (Butun & Sahiner, 2011). The reduction needed 90 min to complete and the K was 0.09 min^{-1}. It took 16 min for the reduction of 4-NP catalyzed by vinyl phosphonic acid–Ni (Sahiner & Sagbas, 2013). To evaluate the recyclability

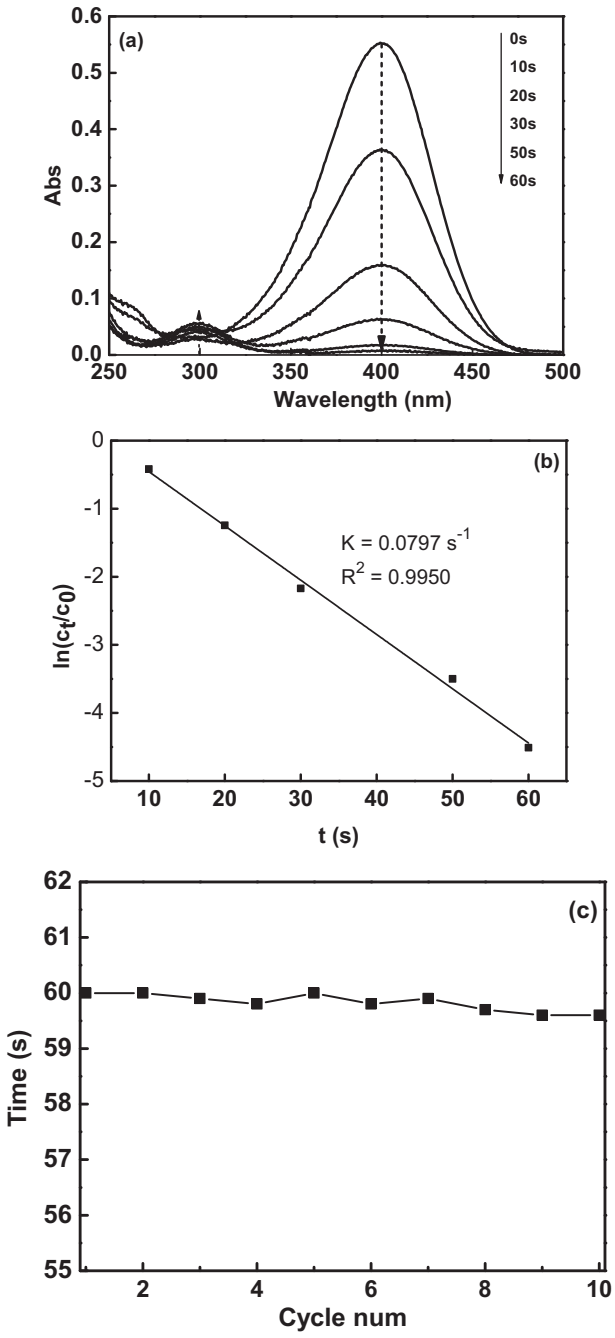

Fig. 8. Successive UV–vis absorption spectra of the reduction of 4-NP by $NaBH_4$ in the presence of Ni@ GO/CMC (a), the ln (c_t/c_0) – t graphs of the reduction of 4-NP (b) and the plot of the reaction time (recording the reaction time when the value of Abs was 1% of the initial value) for ten cycles using Ni@ GO/CMC as the catalyst (c).

of the catalyst, successive cycles of the catalytic reduction were carried out with the Ni@GO/CMC and the results are shown in Fig. 8b. The Ni@GO/CMC can be successfully recycled and reused for at least ten successive cycles without an increase in the reaction time. Thus the Ni@GO/CMC monoliths exhibit good recyclability.

4. Conclusions

Porous GO/CMC monoliths with a unidirectional porous structure were prepared by a green unidirectional freeze-drying method. Their porous structure can be adjusted by changing the composition of the GO/CMC monoliths. The addition of GO greatly

enhanced the mechanical strength of the porous GO/CMC monoliths. The compressive strength increased from 17 kPa (not GO was loaded) to 35 kPa (1% GO was loaded). All the porous CMC and GO/CMC monoliths have high porosities which make the porous monoliths effective adsorbents for heavy metal ions. The Q_e value was different for each ion and was in the order of $Cu^{2+} > Pb^{2+} > Ni^{2+} > Co^{2+} > Cd^{2+}$. When 3% GO was incorporated into the GO/CMC monolith, the Q_e for Pb^{2+} increased from 47.9 (not GO was loaded) to 76.6 mg g^{-1}. In addition, the Ni^{2+} adsorbed on porous GO/CMC monolith was reduced by $NaBH_4$ to obtain the Ni@GO/CMC that exhibited remarkably and stable activity for the catalytic reduction of 4-NP to 4-AP by $NaBH_4$ in aqueous solution. Since CMC is biodegradable, non-toxic and edible, the porous GO/CMC monoliths are potential scaffolds for cell culture and drug delivery.

Acknowledgement

This work was supported by the National Science Foundation of China (21074089 and 21276181).

References

Ali, A. E. H., El-Rehim, H. A. A., Kamal, H., & Hegazy, D. E. S. A. (2008). Synthesis of carboxymethyl cellulose based drug carrier hydrogel using ionizing radiation for possible use as site specific delivery system. *Journal of Macromolecular Science A*, *45*, 628–634.

Balaji, T., El-Safty, S. A., Matsunaga, H., Hanaoka, T., & Mizukami, F. (2006). Optical sensors based on nanostructured cage materials for the detection of toxic metal ions. *Angewandte Chemie International Edition*, *45*, 7202–7208.

Carrington, N. A., Thomas, G. H., Rodman, D. L., Beach, D. B., & Xue, Z. L. (2007). Optical determination of Cr(VI) using regenerable, functionalized sol–gel monoliths. *Analytical Chimica Acta*, *581*, 232–240.

Butun, S., & Sahiner, N. (2011). A versatile hydrogel template for metal nano particle preparation and their use in catalysis. *Polymer*, *52*, 4838–4840.

Cervin, N. T., Aulin, C., Larsson, P. T., & Wågberg, L. (2012). Ultra porous nanocellulose aerogels as separation medium for mixtures of oil/water liquids. *Cellulose*, *19*, 401–410.

Chen, V. J., & Ma, P. X. (2004). Nano-fibrous poly (L-lactic acid) scaffolds with interconnected spherical macropores. *Biomaterials*, *25*, 2065–2073.

Darder, M., Aranda, P., Ferrer, M. L., Gutiérrez, M. C., del Monte, F., & Ruiz-Hitzky, E. (2011). Progress in bionanocomposite and bioinspired foams. *Advance Materials*, *23*, 5262–5267.

Demirbas, A. (2008). Heavy metal adsorption onto agro-based waste materials. *Journal of Hazardous Materials*, *157*, 220–229.

Deville, S., Saiz, E., Nalla, R. K., & Tomsia, A. P. (2006). Freezing as a path to build complex composites. *Science*, *311*, 515–518.

Deville, S., Saiz, E., & Tomsia, A. P. (2007). Ice-templated porous alumina structures. *Acta Materilia*, *55*, 1965–1974.

Dikin, D. A., Stankovich, S., Zimney, E. J., Piner, R. D., Dommett, G. H. B., Evmenenko, G., et al. (2007). Preparation and characterization of graphene oxide paper. *Nature*, *448*, 457–460.

Grzadka, E., & Chibowski, S. (2012). Adsorption and elektrokinetic properties of the system: Carboxymethylcellulose/manganese oxide/surfactant. *Cellulose*, *19*, 23–36.

Gutiérrez, M. C., García-Carvajal, Z. Y., Jobbágy, M., Rubio, F., Yuste, L., Rojo, F., et al. (2007). Poly(vinyl alcohol) scaffolds with tailored morphologies for drug delivery and controlled release. *Advance Functional Materials*, *17*, 3505–3513.

Gutiérrez, M. C., Jobbágy, M., Rapún, N., Ferrer, M. L., & del Monte, F. (2006). A biocompatible bottom-up route for the preparation of hierarchical biohybrid materials. *Advance Materials*, *18*, 1137–1140.

Hummers, W., & Offeman, R. (1958). Preparation of graphitic oxide. *Journal of American Chemistry Society*, *80*, 1339.

Hu, Z., Lei, L., Li, Y., & Ni, Y. (2003). Chromium adsorption on high-performance activated carbons from aqueous solution. *Seperation and Purification Technology*, *31*, 13–18.

Ishaug-Riley, S. L., Crane-Kruger, G. M., Yaszemski, M. J., & Mikos, A. G. (1998). Three-dimensional culture of rat calvarial osteoblasts in porous biodegradable polymers. *Biomaterials*, *19*, 1405–1412.

Kim, J. H., & Lee, T. R. (2004). Thermo and pH-responsive hydrogel-coated gold nanoparticles. *Chemistry of Materials*, *16*, 3647–3651.

Lee, S. B., Kim, Y. H., Chong, M. S., & Lee, Y. M. (2004). Preparation and characteristics of hybrid scaffolds composed of beta-chitin and collagen. *Biomaterials*, *25*, 2309–2317.

Lee, Y. H., Lee, J. H., An, I. G., Kim, C., Lee, D. S., Lee, Y. K., et al. (2005). Electrospun dual-porosity structure and biodegradation morphology of Montmorillonite reinforced PLLA nanocomposite scaffolds. *Biomaterials*, *26*, 3165–3172.

Li, C. B., Wang, X. R., Liu, Y., Wang, W., Wynn, J., & Gao, J. P. (2012). Using glucosamine as a reductant to prepare reduced graphene oxide and its nanocomposites with metal nanoparticles. *Journal of Nanoparticles Research*, *14*, 875.

Matos, G. D., & Arruda, M. A. Z. (2003). Vermicompost as natural adsorbent for removing metal ions from laboratory effluents. *Process Biochemistry*, *39*, 81–88.

Moon, H. J., Ko-du, Y., Park, M. K., Joo, M. K., & Jeong, B. (2012). Temperature-responsive compounds as in situ gelling biomedical materials. *Chemical Society Reviews*, *41*, 4860–4883.

Mukai, S. R., Nishihara, H., Shichi, S., & Tamon, H. (2004). Preparation of porous TiO_2 cryogel fibers through unidirectional freezing of hydrogel followed by freeze-drying. *Chemistry of Materials*, *16*, 4987–4991.

Nishihara, H., Mukai, S. R., & Tamon, H. (2004). Preparation of resorcinol-formaldehyde carbon cryogel microhoneycombs. *Carbon*, *42*, 885–901.

Reddad, Z., Gerente, C., Andres, Y., Thibault, J. F., & Le Cloirec, P. (2003). Cadmium and lead adsorption by natural polysaccharide in MF membrane reactor: Experimental analysis and modeling. *Water Research*, *37*, 3983–3991.

Sahiner, N., & Sagbas, S. (2013). The preparation of poly (vinyl phosphonic acid) hydrogels as new functional materials for in situ metal nanoparticle preparation. *Colloids and Surfaces A*, *418*, 76–83.

Seredych, M., & Bandosz, T. J. (2009). Graphite oxide/AlZr polycation composites: surface characterization and performance as adsorbents of ammonia. *Materials Chemistry and Physics*, *117*, 99–106.

Shunji, Y., Toshiyuki, I., Akio, T., Akira, M., Kazushi, O., Shinichi, S., et al. (2007). Fabrication and mechanical and tissue ingrowth properties of unidirectionally porous hydroxyapatite collagen composite. *Biomedical Materials Research*, *80B*, 166–173.

Soldano, C., Mahmood, A., & Dujardin, E. (2010). Production, properties and potential of graphene. *Carbon*, *48*, 2127–2150.

Stokols, S., & Tuszynski, M. H. (2004). The fabrication and characterization of linearly oriented nerve guidance scaffolds for spinal cord injury. *Biomaterials*, *25*, 5839–5846.

Wang, X. R., Kong, W. N., Xie, W. S., Li, L. Z., Liu, Y., Wu, X. H., et al. (2012). Bi-porous bioinspired chitosan foams with layered structure and their adsorption for xylenol orange. *Chemical Engineering Journal*, *197*, 509–516.

Wan Ngah, S. W., & Hanafiah, M. A. K. M. (2008). Biosorption of copper ions from dilute aqueous solutions on base treated rubber (*Hevea brasiliensis*) leaves powder: Kinetics, isotherm, and biosorption mechanism. *Journal of Environment Science*, *20*, 1168–1176.

Wen, P., Gao, J. P., Zhang, Y. L., Li, X. L., Long, Y., Wu, X. H., et al. (2011). Fabrication of chitosan scaffolds with tunable porous orientation structure for tissue engineering. *Journal of Biomaterials Science Polymer Edition*, *22*, 19–40.

Yang, F., Qu, X., Cui, W. J., Bei, J. Z., Yu, F. Y., Lu, S. B., et al. (2006). Manufacturing and morphology structure of polylactide-type microtubules orientation-structured scaffolds. *Biomaterials*, *27*, 4923–4933.

Yunoki, S., Ikoma, T., Monkawa, A., Ohta, K., Kikuchi, M., Sotome, S., et al. (2006). Control of pore structure and mechanical property in hydroxyapatite/collagen composite using unidirectional ice growth. *Materials Letters*, *60*, 999–1002.

Zhang, H., Long, J., & Cooper, A. I. (2005). Aligned porous materials by directional freezing of solutions in liquid CO_2. *Journal of American Chemical Society*, *127*, 13482–13483.

Zhang, H. F., Hussain, I., Brust, M., Butler, M. F., Rannard, S. P., & Cooper, A. I. (2005). Aligned two- and three-dimensional structures by directional freezing of polymers and nanoparticles. *Nature Materials*, *4*, 787–793.

Zhang, J. N., Huang, Z. H., Lv, R., Yang, Q. H., & Kang, F. Y. (2008). Effect of growing CNTs onto bamboo charcoals on adsorption of copper ions in aqueous solution. *Langmuir*, *25*, 269–274.

Zhang, N. N., Qiu, H. X., Si, Y. M., Wang, W., & Gao, J. P. (2011). Fabrication of highly porous biodegradable monoliths strengthened by graphene oxide and their adsorption of metal ions. *Carbon*, *49*, 827–837.

Zohuriaan-Mehr, M. J., Pourjavadi, A., & Salehi-Rad, M. (2004). Modified CMC. 2. Novel carboxymethylcellulose-based poly (amidoxime) chelating resin with high metal sorption capacity. *Reactive Functional Polymer*, *61*, 23–31.